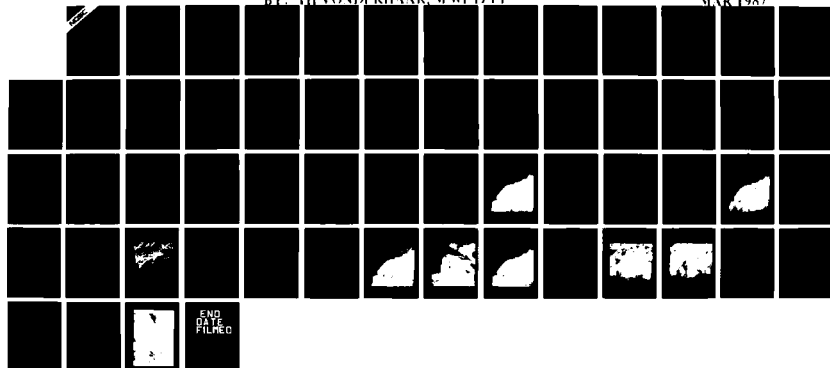


00-0182957

UNCLASSIFIED

NAVAL OCEAN SYSTEMS CENTER, SAN DIEGO, CA  
ESTIMATE OF ELECTRO-OPTICAL METEOROLOGICAL PARA-  
METERS FROM SATELLITE-DETECTED RADIANCES  
BY: HILVONDERHAAR, M WELZLI

FOUO  
NOSC TD 1074  
UNCLASSIFIED  
MAR 1987



**NOSC**

NAVAL OCEAN SYSTEMS CENTER San Diego, California 92152-5000

**Technical Document 1074****March 1987**

# **Estimate of Electro-Optical Meteorological Parameters from Satellite-Detected Radiances**

T. H. Vonder Haar  
M. Wetzel

METSAT, Inc.



Approved for public release; distribution is unlimited

The views and conclusions contained in this report are those of the authors and should not be interpreted as representing the official policies either expressed or implied, of the Naval Ocean Systems Center or the U S Government

# **NAVAL OCEAN SYSTEMS CENTER**

**San Diego, California 92152-5000**

---

**E. G. SCHWEIZER, CAPT, USN**  
Commander

**R. M. HILLYER**  
Technical Director

## **ADMINISTRATIVE INFORMATION**

This work was performed for the Office of Naval Technology, Office of the Chief of Naval Research, Arlington, VA 22217, under program element 62759N. Contract N66001-85-C-0202 was performed by METSAT, Inc., 515 South Howes, Fort Collins, CO 80521.

Released by  
H.V. Hitney, Head  
Tropospheric Branch

Under authority of  
J.H. Richter, Head  
Ocean and Atmospheric  
Sciences Division

UNCLASSIFIED

SECURITY CLASSIFICATION OF THIS PAGE

## REPORT DOCUMENTATION PAGE

1a REPORT SECURITY CLASSIFICATION UNCLASSIFIED			1b RESTRICTIVE MARKINGS	
2a SECURITY CLASSIFICATION AUTHORITY			3 DISTRIBUTION/AVAILABILITY OF REPORT Approved for public release; distribution is unlimited.	
2b DECLASSIFICATION/DOWNGRADING SCHEDULE				
4 PERFORMING ORGANIZATION REPORT NUMBER(S)			5 MONITORING ORGANIZATION REPORT NUMBER(S) NOSC TD 1074	
6a NAME OF PERFORMING ORGANIZATION METSAT, Inc.	6b OFFICE SYMBOL (if applicable)	7a NAME OF MONITORING ORGANIZATION Naval Ocean Systems Center		
6c ADDRESS (City, State and ZIP Code) 515 South Howes Fort Collins, Co 80521		7b ADDRESS (City, State and ZIP Code) Tropospheric Branch San Diego, CA 92152-5000		
8a NAME OF FUNDING SPONSORING ORGANIZATION Office of Naval Technology	8b OFFICE SYMBOL (if applicable) ONT	9 PROCUREMENT INSTRUMENT IDENTIFICATION NUMBER N66001-85-C-0202		
8c ADDRESS (City, State and ZIP Code) Office of the Chief of Naval Research Arlington, VA 22217		10 SOURCE OF FUNDING NUMBERS		
		PROGRAM ELEMENT NO 62759N	PROJECT NO W 59551	TASK NO 540-SXB3
		AGENCY ACCESSION NO DN888 715		
11 TITLE (Include Security Classification) Estimate of Electro-Optical Meteorological Parameters from Satellite-Detected Radiances				
12 PERSONAL AUTHOR(S) T.H. Vonder Haar and M. Wetzel				
13a TYPE OF REPORT Final	13b TIME COVERED FROM Aug 1985 TO Aug 1986	14 DATE OF REPORT (Year, Month, Day) March 1987	15 PAGE COUNT 59	
16 SUPPLEMENTARY NOTATION				
17 COSATI CODES			18 SUBJECT TERMS (Continue on reverse if necessary and identify by block number)	
FIELD	GROUP	SUB GROUP	Electro-optics propagation electromagnetic atmosphere aerosols albedo advanced very high resolution radiometer (AVHRR)	
19 ABSTRACT (Continue on reverse if necessary and identify by block number) This document describes research that includes the implementation of atmospheric transmission models, collection and analysis of digital image data from GOES, DMSP, and NOAA satellites, development of a monochromatic radiative transfer model for marine stratus clouds, and the design and testing of a spectral radiometer for marine boundary layer applications. Summaries of the research project and results are provided in this report. Section 2 describes the analysis of estimating clear-sky atmospheric transmittance from satellite data. Section 3 summarizes the research pertaining to remote sensing applications for boundary layer clouds.				
20 DISTRIBUTION AVAILABILITY OF ABSTRACT <input type="checkbox"/> UNCLASSIFIED, UNLIMITED <input checked="" type="checkbox"/> SAME AS RPT <input type="checkbox"/> DTIC USERS			21 ABSTRACT SECURITY CLASSIFICATION UNCLASSIFIED	
22a NAME OF RESPONSIBLE INDIVIDUAL H. Hughes			22b TELEPHONE (Include Area Code) (619) 225-6520	22c OFFICE SYMBOL Code 543

UNCLASSIFIED

SECURITY CLASSIFICATION OF THIS PAGE (When Data Entered)

[Empty rectangular box for content]

DD FORM 1473, 84 JAN

UNCLASSIFIED

SECURITY CLASSIFICATION OF THIS PAGE (When Data Entered)

## CONTENTS

1.0	Summary .....	1
2.0	Satellite Observations of Clear-Sky Radiance .....	2
	2.1 Sensitivity of LOWTRAN 6 to Boundary Layer Conditions .....	2
	2.2 Correspondence of Satellite and LOWTRAN 6 Radiance .....	5
	2.3 Image Analysis .....	9
3.0	Satellite Observations of Marine Boundary Layer Clouds .....	10
4.0	Summary and Recommendations .....	13
5.0	Acknowledgements .....	14
6.0	References .....	15
	Tables .....	17
	Figures .....	27

## 1.0 SUMMARY

This report describes work completed during the contract period 15 August 1985 - 14 August 1986. The research tasks include the implementation of atmospheric transmission models, collection and analysis of digital image data from the GOES, DMSP, and NOAA satellites, development of a monochromatic radiative transfer model for marine stratus clouds, and the design and testing of a spectral radiometer for marine boundary layer applications. Two field programs have been carried out in collaboration with NOSC in the San Diego area, and data from previous research studies have been incorporated into this research.

Results from portions of the work were published, and these papers were presented at conferences sponsored by the American Meteorological Society and DoD. Summaries of the research project and results are provided in the body of this report, and relevant publications are listed in the References section. Section 2 describes the analysis pursuant to estimating clear-sky atmospheric transmittance from satellite data. Section 3 summarizes the research pertaining to remote sensing applications for boundary layer clouds.

## 2.0 SATELLITE OBSERVATIONS OF CLEAR-SKY RADIANCE

The improvement of the Air Force Geophysical Lab (AFGL) atmospheric transmittance/radiance code (LOWTRAN 6) to include a maritime aerosol model and scattered solar radiation provides the opportunity to intercompare the modeled scene radiance with satellite image data. The objectives of these comparisons are: (1) to evaluate the sensitivity of the LOWTRAN 6 code to local haze and aerosol conditions, (2) to check the correspondence between calibrated satellite radiance and model estimates, and (3) to identify means of enhancing the information content of satellite image data.

### 2.1 Sensitivity of LOWTRAN 6 to Boundary Layer Conditions

Surface meteorological data, sea surface temperatures and atmospheric sounding profiles available for the San Diego area during the 15-18 April 1986 experiment period were used to initialize the LOWTRAN model for shortwave and longwave radiance calculations. The sounding profiles provided by ship-launched balloons off Pt. Loma supplied marine atmospheric parameters up to 500 mb, and the NWS 12-hourly rawinsonde data were applied above this level. The April data set utilized for LOWTRAN is summarized in Table 1.

Direct evaluation of LOWTRAN 6 sensitivity to atmospheric fluctuations were approached by specifying each of the required parameters for the radiance model, and varying those for which some uncertainty was expected. The parameter ICSTL is the most uncertain, since it is a qualitative measure of the prevalence of continental aerosol in the marine boundary layer. If ICSTL is specified to be ten, the aerosol is entirely continental in the size distribution and optical characteristics. ICSTL set equal



to unity infers an entirely marine aerosol layer near the surface (0-2 km). Variations in longwave radiance and visibility calculated with LOWTRAN 6 were found to be sensitive to correct choice of the surface wind speeds and relative humidity in particular. Table 2 provides selected comparisons of these values for varied input parameters. When using observed values of these and the other meteorological inputs, it was estimated that the values for ICSTL should lie between three and five for the April study period in order to reproduce visibility conditions. However, radon measurements obtained from ship indicated that the ICSTL parameter should be scaled to unity, at least for the two-day period of April 15-16. It is difficult to reconcile the calculated visibility under the measured values for ICSTL, surface winds and surface relative humidity. The relatively low visibility of the marine air would seem to require higher relative humidity to be assumed at the surface. The LOWTRAN 6 model should perhaps utilize the higher moisture contents measured above the surface.

Durkee (1986) has provided evidence from a case study of satellite channel radiances that the quantity  $L/E$ , where  $L$  is a shortwave upward-directed radiance and  $E$  is downwelling irradiance, varies with wavelength in a manner that is related to the aerosol population. This quantity is equal to the directional reflectance factor for hemispheric incidence, if multiplied by the constant  $\pi$  steradians. We shall refer to this quantity as directional reflectance ( $DR_\lambda$ ), with the assumption that it is specific to a narrow wavelength region centered on the wavelength  $\lambda$ . Durkee (1986) related the ratio of  $DR_\lambda$  values in the red ( $\lambda = 0.63$  microns) and near-infrared ( $\lambda = 0.86$  microns) satellite channels of the NOAA-7 AVHRR and NIMBUS-7 Coastal Zone Color Scanner (CZCS) to the presence of continental aerosol. We have utilized the atmospheric conditions during the April

field program to calculate radiance in similar wavebands. For later comparison to satellite data collected in April (see Section 2.2), Channel 1 (red) and Channel 2 (near-infrared) wavebands were chosen to match those of the NOAA-6 and the NOAA-9 AVHRR instruments, which are quite close to the NOAA-7 AVHRR channels. The results of the LOWTRAN model calculations in these wavebands are summarized in Table 3 showing the dependence on aerosol characteristics, including aerosol origin, concentration and degree of hydration. Specifying two atmospheric paths in which the 0-2 km boundary layers have equal transmittance at  $\lambda = 0.55 \mu\text{m}$  (equal visibility), but different aerosol populations, the atmosphere with a marine aerosol layer has a notably lower near-infrared (NIR) radiance, while the red-waveband radiance is only slightly less than in the case of a rural aerosol population. For the afternoon conditions observed on April 18 during the field experiment period, and assuming marine aerosol and a 23 km visibility, NIR radiance is  $0.29 \text{ mWcm}^{-2}\text{sr}^{-1}$  while red radiance is  $0.42 \text{ mWcm}^{-2}\text{sr}^{-1}$ , and the ratio of radiances for red vs. NIR is 1.45 for the marine aerosol, while it is 1.62 for the assumption of a rural aerosol composition. Relative humidity effects are manifest through absorption of near-infrared radiation in the presence of any aerosol, and through shortwave extinction by haze droplets in the presence of the deliquescent marine aerosol. For example, a shift in the surface relative humidity from 88% to 68% for an entirely rural aerosol population decreases the red/NIR radiance ratio, primarily by increasing NIR transmittance. For comparisons such as these, the radiance ratio is sufficient, since the second multiplicative term in the expression for the  $\text{DR}_\lambda$  ratio is the NIR/red downward irradiance ratio, which will be a constant. Quantitative comparison of  $\text{DR}_\lambda$  ratios in the satellite channels is accomplished below.

## 2.2 Correspondence of Satellite and LOWTRAN 6 Radiance

NOAA-6 and NOAA-9 satellite data from the Advanced Very High Resolution Radiometer (AVHRR) imager were archived during the period 15-18 April (see Table 4) from which the upwelling radiances observed at satellite position were determined. Subsets of these data are provided for the study region in Figures 1-5. These radiances were then compared to results of LOWTRAN 6 model calculations, by incorporating the boundary layer and free atmosphere contributions, as described in Section 2.1, for times matching the satellite overpass.

The satellite-observed radiance has been modeled for the viewing geometry of the polar-orbiting satellites determined from orbit parameters provided by the Scripps Satellite Oceanography Facility (SSOF). LOWTRAN 6 results were compared to satellite data by two procedures. First, spectral radiance from LOWTRAN at a specific central wavelength was matched against the equivalent-blackbody radiance of the satellite thermal channels. The central wavelength was chosen to be that at which the satellite channel calibrations had been performed, for the observed temperature range. AVHRR channel calibration is determined for monochromatic wavelengths only, and this is a central wavelength rather than the peak transmittance wavelength. For example, peak transmittance for NOAA-9 AVHRR Channel 4 is found at 10.50 microns, while radiance calibration is valid at 10.76 microns, near the center of the filter bandpass.

A second procedure was utilized for analysis of shortwave radiance, based on the channel calibration with respect to scene albedo over the entire bandpass. The LOWTRAN 6 filter function subprogram, LOWFIL, provided the means to estimate albedo.

To quantitatively test the observed and calculated radiances, the signal conversion procedure specified for AVHRR shortwave channels must be followed. A pre-launch laboratory calibration of the Channel 1 and Channel 2 sensors provides the following conversion for channel radiance,  $L_{f\lambda}$ ;

$$L_{f\lambda} = \frac{A_{\lambda} \cdot E_{f\lambda}}{\pi}, \quad (1)$$

where the albedo ( $A$ ) of the satellite channel centered at wavelength  $\lambda$  is given by a linear relationship to pixel brightness, and  $E_{f\lambda}$  is the sensor-weighted solar irradiance on a horizontal surface at the top of the atmosphere.  $E_{f\lambda}$  was obtained by integrating solar irradiance with the channel filter functions (transmittance curves) in narrow wavelength intervals across the filter bands (0.53 - 0.80  $\mu\text{m}$  for Channel 1, 0.69-1.125  $\mu\text{m}$  for Channel 2). For the LOWTRAN radiance 0.15  $\text{mWcm}^{-2}\text{sr}^{-1}$ , Channel 2 pixel albedo should be 2.4%. Satellite-observed albedos at the location and viewing geometry for which the model calculations were performed (on the morning of April 18, directly off Pt. Loma in the area shown by Figure 6) equal only 1.7%. The satellite image albedos are also less than predicted values for Channel 1, and at other image times deviations of up to 1% also are noticed. Table 5 lists Channel 1 and 2 albedos at the study location observed by NOAA-9 and calculated by LOWTRAN. Images corresponding to the three individual cases are presented in Figures 2d, 7 and 8. For the April 16 case, observed satellite radiances for Channel 2 lie in the visibility range where aerosol type (marine vs. continental) has only a small impact on extinction. The location of the value of observed radiance would lead to a visibility estimate from the plotted curves similar to that which was recorded. Again, however, the data used to plot these curves would require

a high relative humidity to produce this value. Sensitivity of model results to ocean surface albedo is not sufficient to account for the difference. Although the source of the deviation could be due to instrument response or model error, it is small in magnitude. The values of the bi-spectral brightness ratios are consistent between model results and satellite data. The ratio of scaled radiances in Channels 1 and 2 can be evaluated from the satellite data as the ratio of albedos in Channels 1 and 2. Following Eqn. 1, the value of  $A_{\lambda_1}/A_{\lambda_2}$  would be expected to increase with the predominance of continental aerosol for a given value of optical depth. The ratio  $(DR_{\lambda_1}/DR_{\lambda_2})$  for the NOAA-6 April 18 morning satellite pass time case is 1.30 from satellite data alone and 1.37 from model calculations, showing agreement within 1% for the ratio value.

Calculations of narrow-band radiance in the longwave channels also demonstrate agreement between LOWTRAN 6 and calibrated AVHRR data. For each of the satellite channels, the digital pixel brightness is directly related to an equivalent-blackbody temperature. The radiance associated with this value is recovered simply by using the Planck blackbody function. Pixel radiance values may be expected to equal upwelling radiance computed from the transmission model, assuming the viewing geometry and meteorological parameters are accurately specified. The NOAA-9 Channel 4 calibrated radiance at the Pt. Loma Waypoint #1 on April 16 (satellite image is enhanced to emphasize haze in Figure 4d) was  $0.79 \text{ mWcm}^{-2}\text{sr}^{-1}$ , while LOWTRAN 6 calculations for the same waveband produced approximately  $0.74 \text{ mWcm}^{-2}\text{sr}^{-1}$  (see Table 2). Variations in the viewing geometry within the area, from Waypoint #1 to #9 (a distance of 0.25 degrees longitude) amount to only 0.1% of the calculated radiance. Another case study, on the afternoon of April 17, again showed NOAA-9 Channel 4 radiance ( $0.80 \text{ mWcm}^{-2}\text{sr}^{-1}$ )

within 4% of model radiance ( $0.77 \text{ mWcm}^{-2}\text{sr}^{-1}$ ). Enhanced imagery for this case is displayed in Figure 10. Results for Channels 3 ( $3.7 \mu\text{m}$ ) and 5 ( $11.8 \mu\text{m}$ ) are given in Tables 6 and 7.

It was determined from the results of many LOWTRAN output comparisons that the incorporation of accurate sounding profiles above 500 mb was not significant to the accuracy of these case studies. Estimation of surface relative humidity and surface winds are critical in predicting the concentration of haze droplets. The uncertainty in sea surface temperature is unimportant, as discussed below.

The parameterization recommended by NOAA (Kidwell, 1985) for daytime determination of sea surface temperature (SST) from the AVHRR digital image data utilizes the Channel 4 ( $10.76 \mu\text{m}$  center wavelength) and Channel 5 ( $11.85 \mu\text{m}$  center wavelength). For example, using NOAA-9 AVHRR data,

$$\text{SST } (^{\circ}\text{C}) = 3.6569 T_4 - 2.6705 T_5 - 268.92, \quad (2)$$

where  $T_4$  is the calibrated equivalent-blackbody temperature (in degrees Kelvin) for Channel 4, and  $T_5$  is that for Channel 5. The difference in brightness temperatures between these two channels is a measure of atmospheric moisture.  $T_5$  is less than  $T_4$  under normal circumstances. From SST measured at Pt. Loma, observations during the period 15-17 April ranged  $62^{\circ}\text{F}$  ( $17^{\circ}\text{C}$ ) to  $68^{\circ}\text{F}$  ( $20^{\circ}\text{C}$ ). Upwelling radiance defined merely by equivalent-blackbody temperatures varies by a few percent across this range, but radiance leaving the atmosphere from an ocean surface with this temperature variation is relatively constant. Comparing the satellite-derived SST for NOAA-9 pass times on April 17 (Figure 10) and April 18 (Figure 11), a variation of only  $0.6^{\circ}\text{C}$  is noted. At the same conditions, LOWTRAN estimates show Channel 4 radiances to vary from  $0.77$  to

0.87 mWcm<sup>-2</sup>sr<sup>-1</sup>. This is assumed to be caused by the 24-hour change in boundary layer haze conditions due to modification of the air mass through windspeed fluctuations, relative humidity changes, or alteration of the specified aerosol origin. The observed or probable SST fluctuations would not produce changes of this magnitude in the satellite channel radiances.

### 2.3 Image Analysis

Modifications to the marine haze layer are manifest in the results of LOWTRAN 6 radiance calculations at visible, near-infrared and thermal wavelengths simultaneously, through changes in the size-dependent number concentrations and extinction properties of aerosol.

The comparisons of satellite radiances in the shortwave and longwave channels to LOWTRAN calculations that were described in the previous section show that the model provides sufficient accuracy and sensitivity to study image patterns produced by haze variations. The LOWTRAN results also display smooth variation with zenith angle toward the horizon (except very near 0° elevation), as shown in the solid lines of Figure 12.

Unfortunately, narrow-band radiometric observations taken simultaneously by the Spectral Radiometer located at Pt. Loma were too noisy (vertical bars) to draw any definite conclusions on a correspondence to model results. The interrelationship of horizontal path transmittance to upwelling radiance variations should be explored further. Time-series studies of enhanced GOES and NOAA satellite data from the field projects reveal areas of haze for which the horizontal transmittance could be measured from a ship-based or land-based filter radiometer.

### 3.0 SATELLITE OBSERVATIONS OF MARINE BOUNDARY LAYER CLOUDS

Research under this topic has been described in the two papers previously submitted (Wetzel and Vonder Haar, 1986a, 1986b), and will be summarized below. It is evident from routine satellite imagery that marine stratus cloud is maintained over large regions by synoptic-scale forcing, but that convective motions on the cloud scale are also necessary. Local energy budgets are therefore a critical factor in governing cloud development and dissipation. The growth of haze droplets due to radiative cooling may lead to cloud formation, and the absorption of solar energy by cloud contributes to the net energy balance in rising parcels at cloud top. The size of droplets with these cloudy parcels determines both their radiative and microphysical interactions with the environment.

A technique proposed for determination of cloud droplet size parameters, using satellite remote sensing, employs the shortwave bands where water vapor absorption is small. The results of multiple scattering radiative transfer calculations demonstrate that directional reflectance in the NIR vapor window at  $1.6 \mu\text{m}$ , for example, is reduced measurably when the effective radius of the cloud layer droplet population is increased. The effective radius is a ratio of volume-weighted to cross-section-weighted number concentrations for cloud droplets, which provides a parameter that scales the relationship of droplet absorption versus scattering processes.

It is suggested that a satellite sensor designed for this application should provide NIR window radiances simultaneously in at least two channels, with one near the visible ( $0.85 \mu\text{m}$ ) to estimate the scaled optical depth of the stratus layer. Figure 13 shows the direct relationship of scaled optical depth to  $0.85 \mu\text{m}$  reflectance, while Figure 14 is an example



of how 0.85  $\mu\text{m}$  reflectance can then be used to discriminate the 1.6  $\mu\text{m}$  reflectance variations due to droplet size. Several tests have been carried out with the multiple scattering model to simulate remote sensing of multi-layer clouds. The optical depth, droplet characteristics near cloud top, and viewing geometry all are significant factors of cloud reflectance, but can be separated through numerical experiment. We have also designed and field-tested a remote sensing system to measure spectral radiance in the NIR windows centered at 0.85, 1.6, and 2.2 micron wavelengths. The schematic design of the Discrete Filter Wheel implemented for this study is shown in Figure 15. The Spectral Radiometer System was operated as part of cloud microphysics-radiation experiments in collaboration with NOSC during April and June, 1986. Data from the June aircraft flights show the cloud-scale fluctuations in upward-directed spectral radiance expected in the shortwave bands. Analysis of the data sets for reflectance signatures that are related to microphysical conditions is ongoing. An example of the raw data captured during the research flights in June is presented in Figure 16, where the vertical scale is proportional to measured radiance in each channel, and the horizontal scale represents fractions of seconds along an aircraft flight leg. A complete study of the results from the summer experiment will include combined evaluation of the satellite, radiometer and microphysical data sets.

Digital imagery available from a DMSP Special Sensor C (SSC) experiment during a short period in 1979 provides the only satellite observations of clouds in a near-infrared window band. Figure 17 is an example set of images in the visible, near-infrared (SSC), and thermal window for an ocean region off the East Coast. The ability of multi-spectral techniques to discriminate low water cloud from ice cloud is obvious by comparing the

brightness of the three images for the high frontal cloud band in the center of the image. The value of the Special Sensor image for studying the stratocumulus cloud field near the top of the image is not obvious. While the radiative transfer calculations indicate cloud reflectance should be lower for the SSC than the visible channel, the effects due to coarse resolution and broken cloud fields are difficult to assess. Remote sensing studies from aircraft should be continued for the stratus applications, particularly because these simultaneously provide the aerosol/droplet sampling, as well as the radiometric observations at higher resolution than satellites currently allow.

#### 4.0 SUMMARY AND RECOMMENDATIONS

The research project during the past year has allowed us to extend the results of previous studies on satellite applications, particularly with regard to intercomparison with standard atmospheric transmittance models. It has also been possible to study the basis of a new technique for characterizing marine layer clouds, so that their evolution may be related to the near-cloud environmental parameters. A wider range of meteorological scenarios must be routinely sampled with the radiometric instrumentation available and coincident satellite-based imagers to allow improvement of and reliance on the numerical models during image interpretation. The multiple-scattering radiative transfer methods can then be meshed with LOWTRAN to provide cloudy-clear air analyses.

## 5.0 ACKNOWLEDGEMENTS

The successful completion of the aircraft field program described in Section 3 was only possible through the expertise contributed by Dr. Doug Jenson of NOSC, to whom the authors are indebted. Appreciation is extended to Dr. Herb Hughes of NOSC, Dr. Phil Durkee of the Naval Postgraduate School and the Gibbs Flying Service for their support. Other contributions were made by Hung-Chi Kuo, Jan Behunek and Chris Johnson-Pasqua of Colorado State University. Discussions with Dr. Steve Cox of CSU on various research aspects are also gratefully acknowledged.

## 6.0 REFERENCES

- Durkee, P.A., 1986: Aerosol characterization with dual-wavelength radiance measurements. Preprints, AMS Second Conference on Satellite Meteorology/Remote Sensing and Applications, 13-16 May 1986, Williamsburg, VA, 298-302.
- Kidwell, K. B., 1985: NOAA Polar Orbiter Data Users Guide. National Oceanic and Atmospheric Administration, Washington, DC.
- Kneizys, F. X., E. P. Shettle, W. O. Gallergy, J. H. Chetwynd, Jr., L. W. Abreu, J. E. A. Selby, S. A. Clough and R. W. Fenn, 1983: Atmospheric transmittance/radiance: Computer code LOWTRAN 6. AFGL-TR-83-0187, Hanscom AFB, MA, 200 pp.
- Vonder Haar, T. H., 1985: Progress Report #1 to Naval Ocean Systems Center, Contract N66001-86-R-0202. METSAT, Inc., 1 p.
- Vonder Haar, T. H., 1986a: Progress Report #2 to Naval Ocean Systems Center, Contract N66001-86-R-0202. METSAT, Inc., 4 pp.
- Vonder Haar, T. H., 1986b: Progress Report #3 to Naval Ocean Systems Center, Contract N66001-86-R-0202. METSAT, Inc., 1 p.
- Wetzel, M. and T. H. Vonder Haar, 1986a: The impact of stratocumulus microphysical variations on near-infrared radiance. Extended abstracts, AMS Sixth Conference on Atmospheric Radiation, 12-16 May 1986, Williamsburg, VA, 153-156.
- Wetzel, M. and T. H. Vonder Haar, 1986b: Modeling and observation of near-IR cloud signatures in the marine boundary layer. DoD Fourth Tri-Service Cloud Modeling Workshop, 3-4 June 1986, Janscom AFB, MA 50-64.

TABLES

TABLE 1. Data Set for LOWTRAN Model Calculations

<u>Data Source</u>	<u>Description</u>	<u>Date/Time(GMT)</u>
NOSC	Vertical profiles from ship-launched balloons, near Pt. Loma	16 Apr 86/0345 /1645 /2045 17 Apr 86/0045
NWS	12-hourly rawinsonde profiles from Montgomery Field	15 Apr 86/1200- 19 Apr 86/0000
NOSC	Pt. Loma surface observations (inc. sea surface temperature)	15 Apr 86/2230- 16 Apr 86/0510  16 Apr 86/1530- 16 Apr 86/1700  16 Apr 86/2000- 16 Apr 86/2100  16 Apr 86/2345- 17 Apr 86/0130
NWS	Hourly surface observations at San Diego, Lindbergh Field, San Nicholas Island and North Island	15 Apr 86/1200- 19 Apr 86/0200

TABLE 2. LOWTRAN Model Parameters and Results for the 10-11  $\mu\text{m}$  band.

Time (GMT)	Surface Relative Humidity (%)	ICSTL (n.d.)	Current Wind Speed (m/s)	24-hour Average Wind Speed (m/s)	Visibility (km)	10.76 $\mu\text{m}$ Radiance ( $\text{mWcm}^{-2}\text{sr}^{-1}\mu\text{m}^{-1}$ )
0045	* 50	1	10.3	7.7	32.7	0.75
(17 April)	60	1	10.3	7.7	27.0	0.74
	60	1	9.8	7.7	28.1	0.75
	60	1	7.7	7.7	33.4	0.76
	60	1	1.7	7.7	66.0	0.80
	60	1	10.3	5.1	31.9	0.74
	60	2	2.6	7.7	57.3	0.80
	60	3	10.3	7.7	24.8	0.74
	60	5	9.8	7.7	21.8	0.75
	65	2	7.7	7.7	29.3	0.76
	70	1	7.7	7.7	28.2	0.76
	70	2	7.7	7.7	26.8	0.76
	75	2	7.7	7.7	24.8	0.75
	98	1	10.3	7.7	2.9	0.47
2045	* 50	2	10.3	6.2	34.6	0.74
(16 April)	65	1	10.3	6.2	27.1	0.73
	65	2	10.3	6.2	26.1	0.73
	75	2	7.7	7.7	24.8	0.75
1645	* 65	1	4.6	6.2	50.1	0.77
(16 April)	75	1	4.6	6.2	43.1	0.77
	85	1	4.6	6.2	38.8	0.77

Notes: Upper air temperature and humidity data obtained from radiosonde ascents for 16 April 1986. Parameter lists marked by an asterisk(\*) represent observed surface conditions of relative humidity, ICSTL, and winds for the time period indicated. Calculated visibilities are greater than those measured at 1645 GMT (18.5 km), 2045 (27.7 km), and 0045 (18.5 km).



TABLE 3. LOWTRAN Model Parameters and Results for NOAA-9 AVHRR  
Channels 1 and 2

Time (GMT)	Channel Number	Surface Relative Humidity (%)	ICSTL (n.d.)	Current Wind Speed (m/s)	24-hour Average Wind Speed (m/s)	Visibility (km)	Filter-Integrated Radiance ( $\text{mWcm}^{-2}\text{sr}^{-1}$ )
0045 (17 April)	1	60	1	10.3	7.7	27.1	0.163
	1	60	2	7.7	7.7	32.0	0.158
	1	60	5	10.3	7.7	21.2	0.171
	1	75	2	7.7	7.7	24.8	0.166
.	2	60	1	1.7	7.7	66.0	0.104
	2	60	3	10.3	7.7	24.8	0.141
	2	60	5	10.3	7.7	21.2	0.147
	2	60	5	7.7	7.7	24.9	0.137
	2	60	5	1.7	7.7	39.5	0.113
	2	70	1	10.3	7.7	26.8	0.139
	2	70	1	7.7	7.7	28.1	0.137
	2	70	1	7.7	10.3	23.7	0.145
	2	70	1	5.1	10.3	29.7	0.134
	2	70	5	10.3	5.1	19.5	0.150
	2	75	2	7.7	7.7	24.8	0.142
	2	80	5	10.3	7.7	14.4	0.170
	2	95	1	10.3	7.7	10.1	0.202
	2	95	5	10.3	7.7	6.3	0.215
	2	98	1	10.3	7.7	2.9	0.239
	2	98	5	10.3	7.7	1.5	0.247

TABLE 4. NOAA AVHRR Data Archived For April Experiment

<u>Satellite</u>	<u>Date/Time(GMT)</u>
NOAA-9	April 15/2227
NOAA-6	April 16/0246
NOAA-9	April 16/2216
NOAA-6	April 17/1442
NOAA-9	April 17/2205
NOAA-6	April 18/1418
NOAA-9	April 18/2155

TABLE 5. LOWTRAN model parameters and results for NOAA-9  
AVHRR Channels 1 and 2

Time (GMT)	Channel Number	Surface Relative Humidity (%)	ICSTL (n.d.)	LOWTRAN Albedo (%)	Satellite Albedo (%)
2227 (15 April)	1	70	1	3.2	3.0
	2	70	1	2.0	1.0
2216 (16 April)	1	75	2	2.9	3.4
	2	75	2	1.9	2.1
2205 (17 April)	1	50	1	2.0	3.2
	2	50	1	1.3	1.7

TABLE 6. LOWTRAN Model Parameters and Results for NOAA-9  
AVHRR Channel 3.

Time (GMT)	Surface Relative Humidity (%)	ICSTL (n.d.)	Current Wind Speed (m/s)	24-hour Average Wind Speed (m/s)	Visibility (km)	3.73- $\mu$ m Radiance ( $\text{mWcm}^{-2}\text{sr}^{-1}\mu\text{m}^{-1}$ )
0045	60	1	10.3	7.7	27.0	0.027
(17 April)	60	1	5.1	7.7	43.5	0.028
	60	5	10.3	7.7	21.2	0.027
	80	1	10.3	7.7	19.7	0.026
	95	1	10.3	7.7	10.1	0.022

Note: Satellite radiance for 2216 GMT (16 April) pass is  $0.026 \text{ mWcm}^{-2}\text{sr}^{-1}\mu\text{m}^{-1}$  at  
Way Point #1 near Pt. Loma.

TABLE 7. LOWTRAN Model Parameters and Results for NOAA-9  
AVHRR Channel 5.

Time (GMT)	Surface Relative Humidity (%)	ICSTL (n.d.)	Current Wind Speed (m/s)	24-hour Average Wind Speed (m/s)	Visibility (km)	11.8- $\mu$ m Radiance ( $\text{mWcm}^{-2}\text{sr}^{-1}\mu\text{m}^{-1}$ )
0045	50	2	5.1	7.7	49.7	0.75
(17 April)	60	1	10.3	7.7	27.0	0.72
	60	5	10.3	7.7	21.2	0.71
	80	1	10.3	7.7	19.7	0.70

Note: Satellite radiance for 2216 GMT (16 April) pass is  $0.72 \text{ mWcm}^{-2}\text{sr}^{-1}\mu\text{m}^{-1}$  at  
Way Point #1 near Pt. Loma.

FIGURES







[illegible]

31





[illegible]

34

241 498 141 398 1.0 1.0 1 1 N9106PM2E.IMG N-9 ENHANCED CHANNEL 2



Fig. 2(d) Enhanced satellite image, showing area of three adjacent panels in the Fig. 2(a)-2(c) in center, and surrounding region.





C



241 498 141 396 1.0 1.0 1 0 N9108PM3E.IMG N-9 ENHANCED CHANNEL 3



Fig. 3(d). Enhanced satellite image for Channel 3, showing area of Fig. 3(a)-3(c) and surrounding region.



[illegible]

Fig. 4(b). Channel 4, central panel.



241 456 141 3.3 1.0 1.0 1 1 N9106PM4E.IMG N-9 ENHANCED CHANNEL 4



Fig. 4(d). Enhanced satellite image for data shown in Fig. 4(c) and surrounding region.

Bandpass is 11.25 - 12.65 microns

NY 61-11 1A 221A7 CH.5

[illegible]

Fig. 50. A in Fig. 1, for Channel 5 data.

[illegible]







241 496 141 396 1.0 1.0 1 1 N6108AM2E.IMG N-6 ENHANCED CHANNEL 2

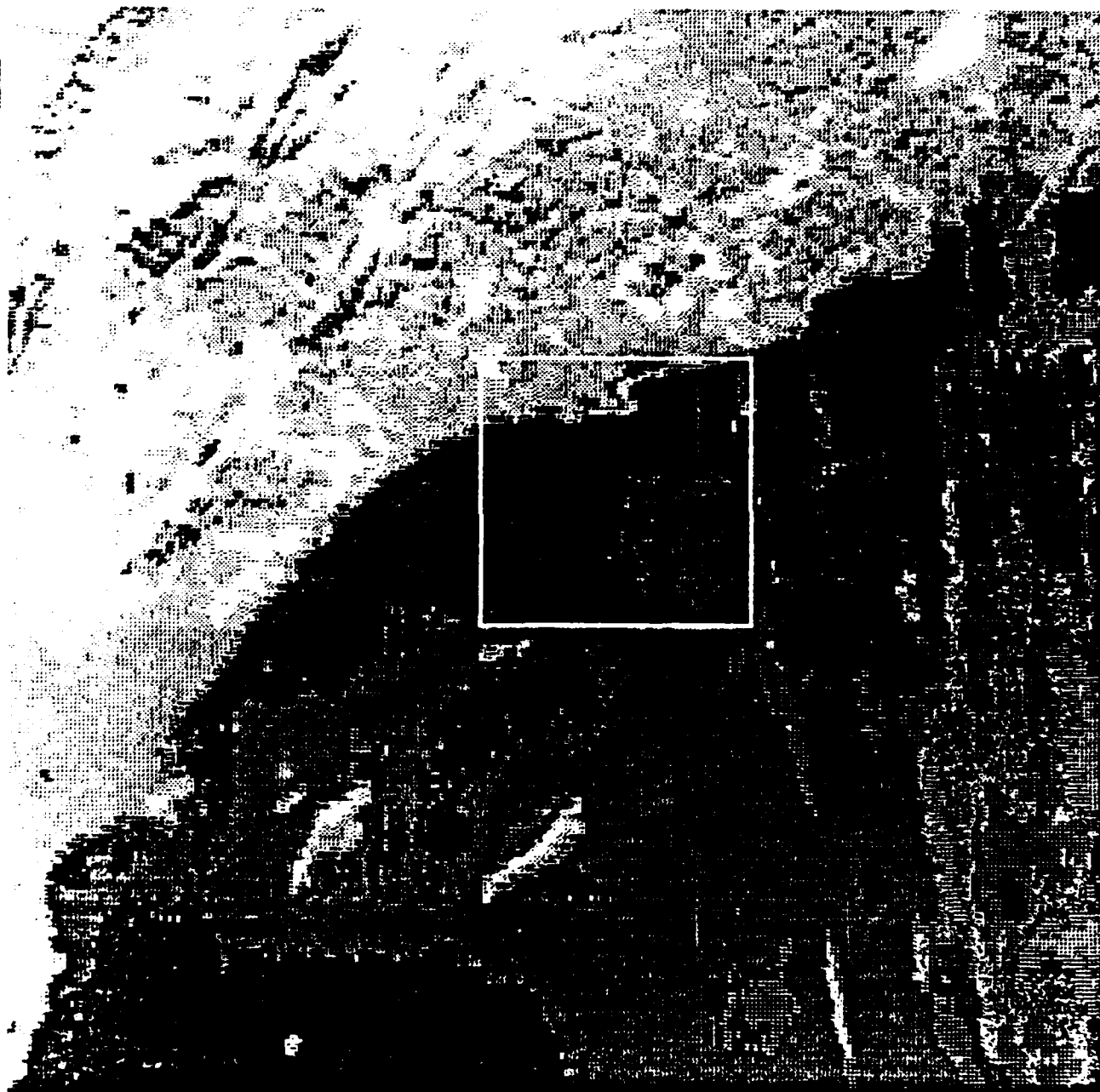


Fig. 6. Enhanced satellite image, showing immediate study area.

51 308 51 308 1.0 1.0 1 1 N9105PM2E.IMG N-9 ENHANCED CHANNEL 2

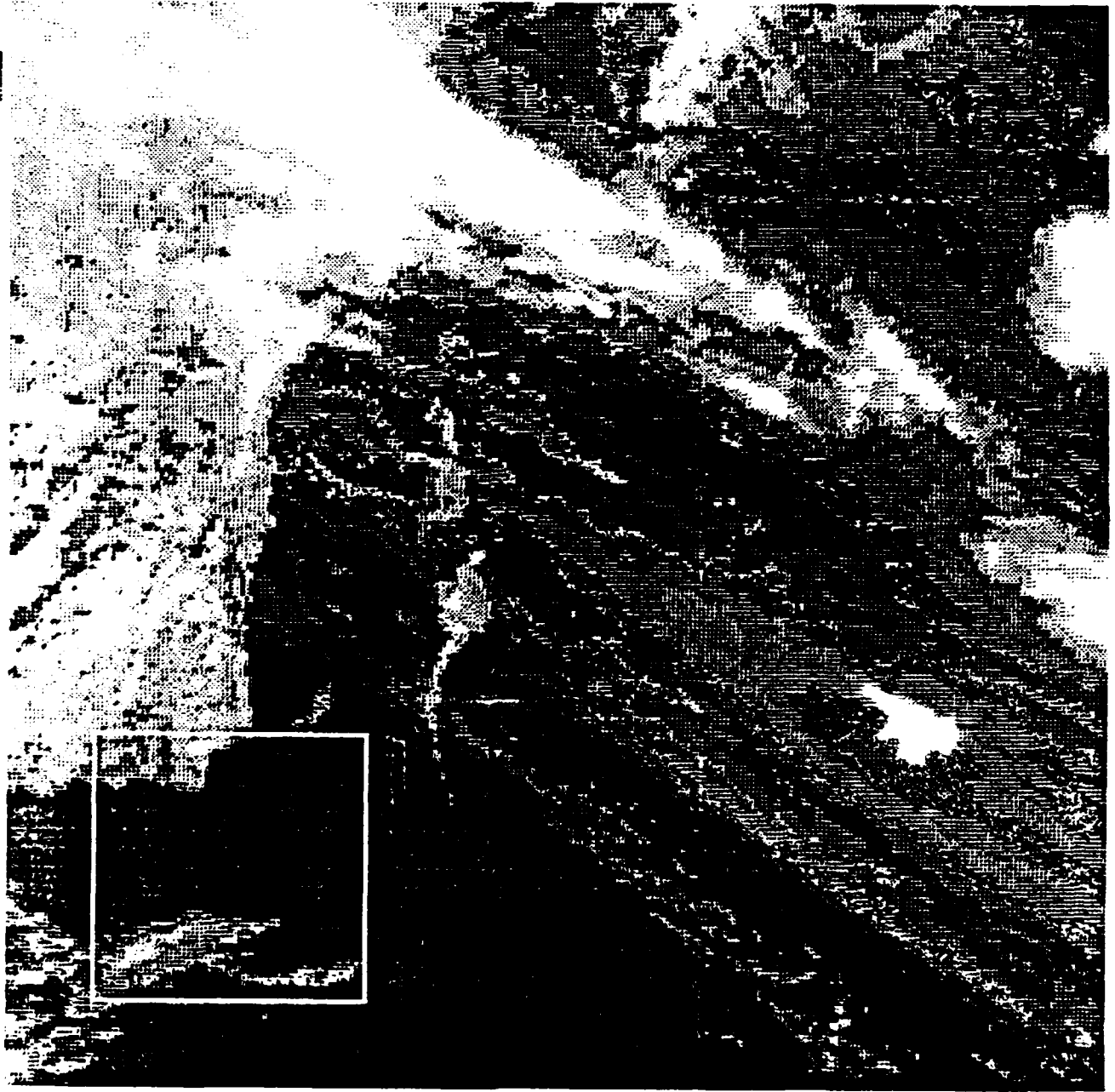


Fig. 7., Enhanced satellite image for 15 April NOAA-9 pass, showing area of pixel sampling within box.

241 498 141 398 1.0 1.0 1 1 N9107PM2E.IMG N-9 ENHANCED CHANNEL 2



Fig. 8. Enhanced satellite image for 17 April NOAA-9 pass.

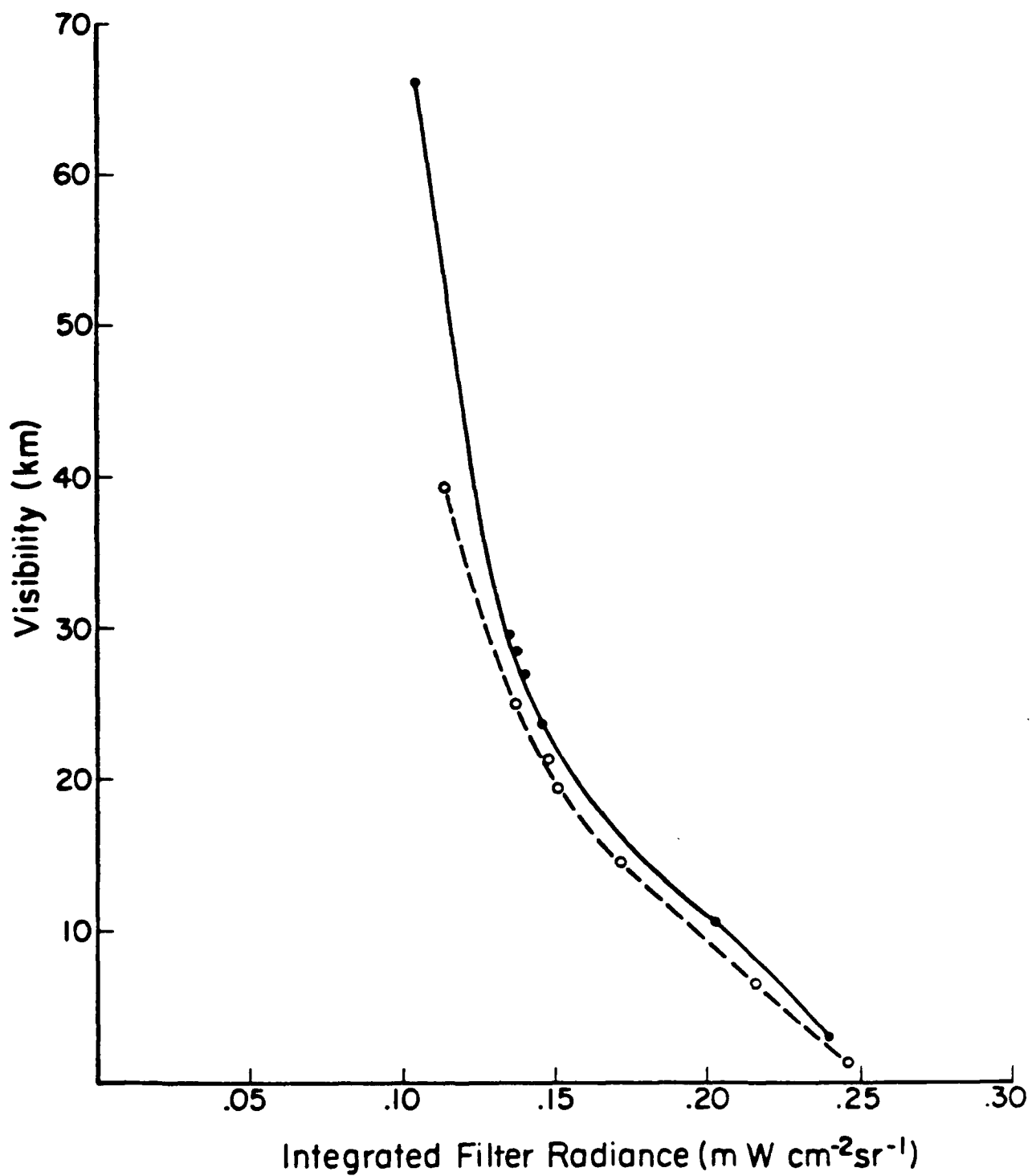


Fig. 9. Radiance calculated by LOWTRAN 6 for AVHRR Channel 2 (near-infrared) and resultant visibility for a range of surface meteorological conditions. Values of ICSTL parameter are 1 for solid circles, and 5 for open circles. Lines represent hand-drawn curves connecting the values.

241 496 141 396 1.0 1.0 1 1 N9107PM4E.IMG N-9 ENHANCED CHANNEL 4



Fig. 10. Enhanced satellite image for 17 April NOAA-9 pass (Channel 4).

241 496 141 396 1.0 1.0 1 1 N9108PM4E.IMG N-9 ENHANCED CHANNEL 4



Fig. 11. Enhanced satellite image for 18 April NOAA-9 pass (Channel 4).

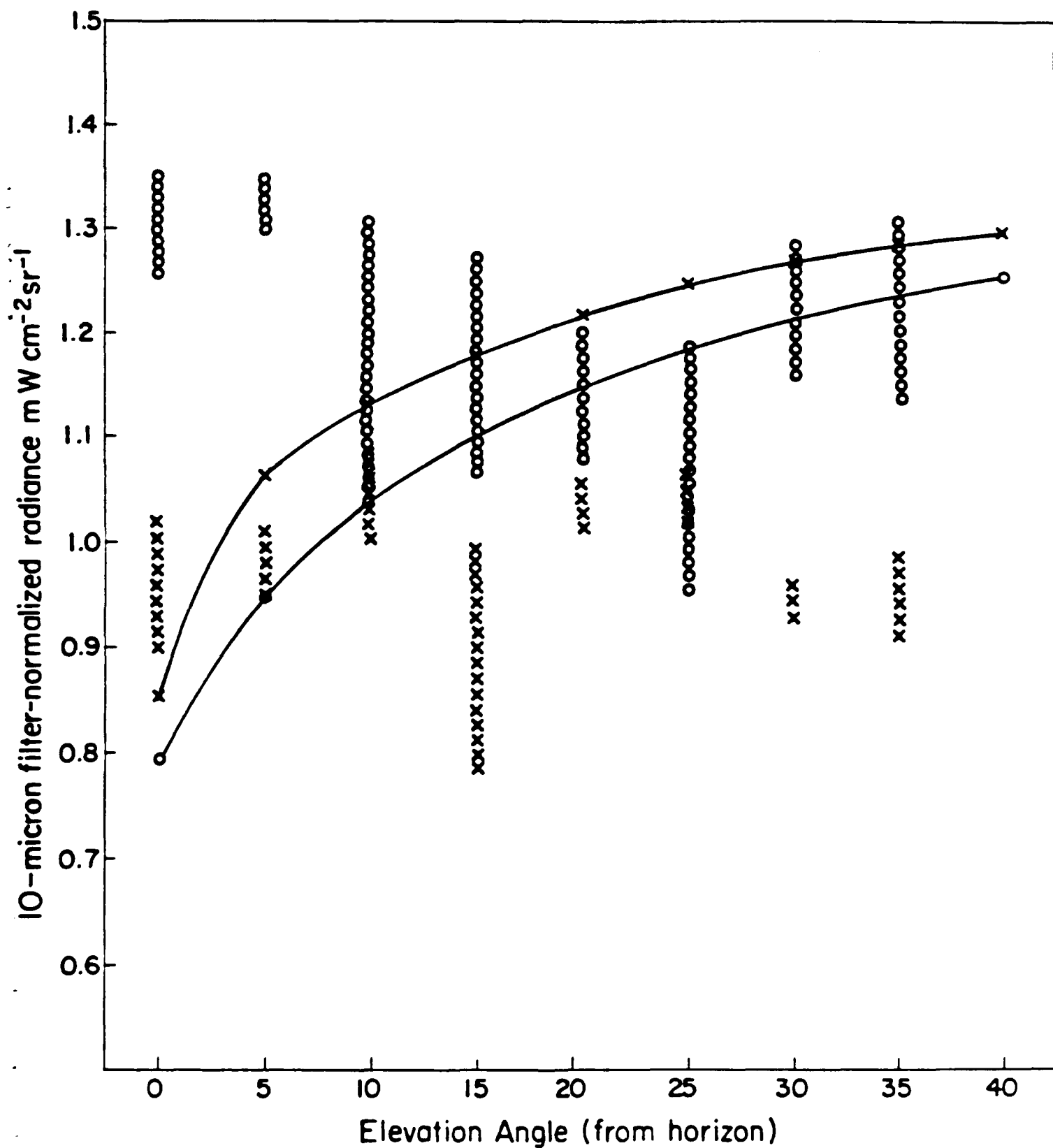


Fig. 12. LOWTRAN 6 radiance calculations for the 10-micron filter band (solid curves) used to obtain Spectral Radiometer clear air measurements (range of values shown in vertical bars of X and O symbols). X refers to data from 18 April; O for 16 April.

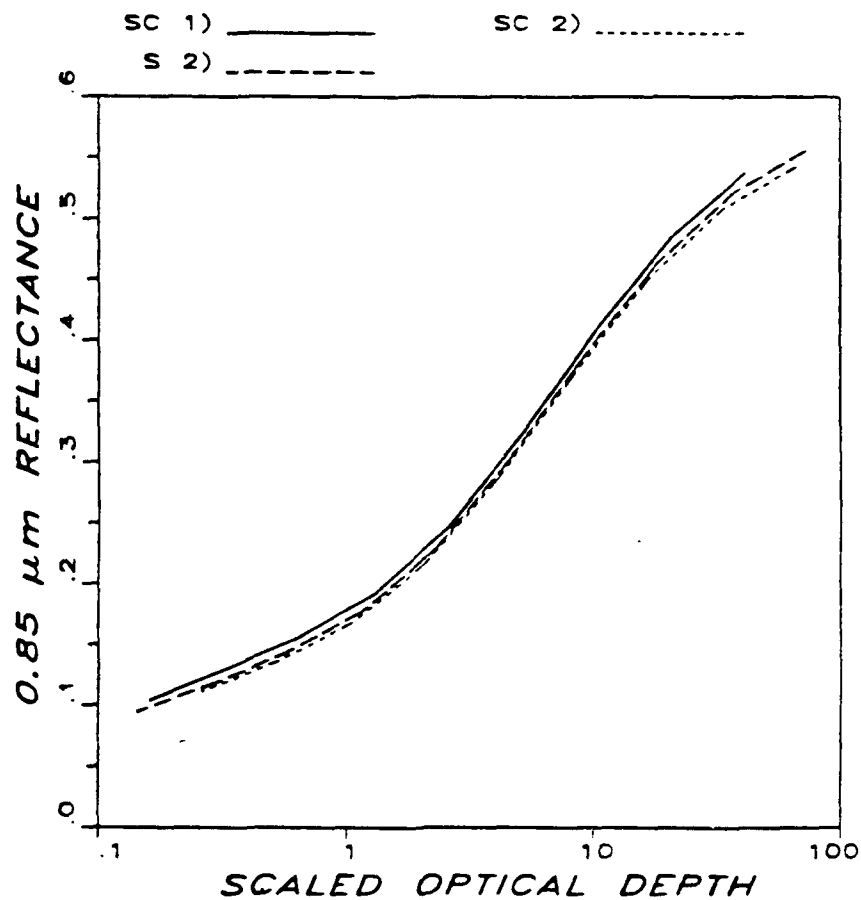


Fig. 13. Reflectance calculated for three different model cloud layers.

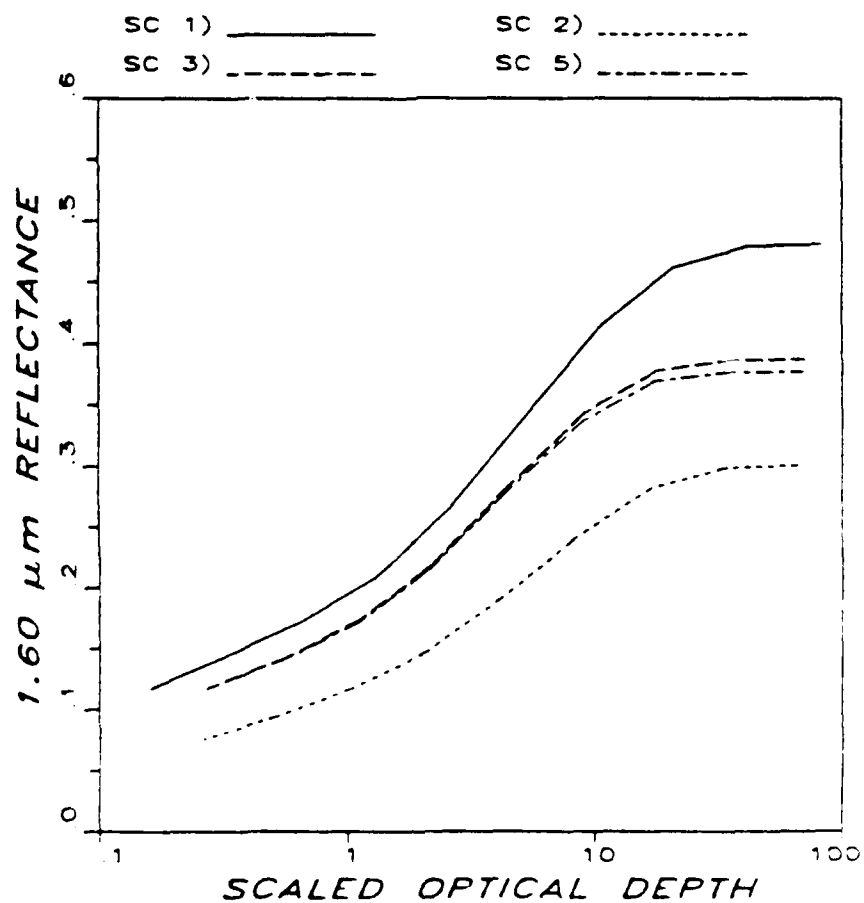


Fig. 14. 1.60- $\mu\text{m}$  reflectance calculated for different model cloud layers.



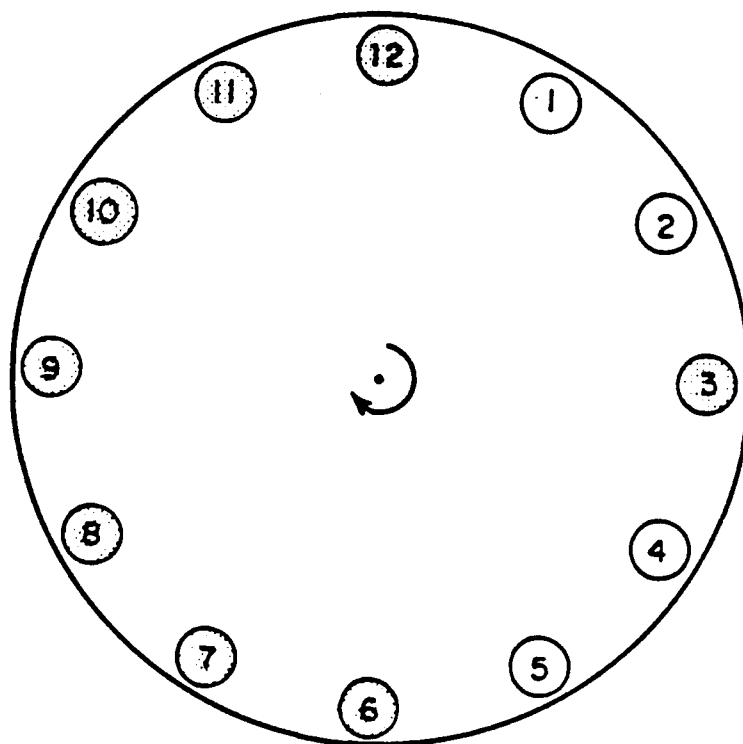


Fig. 15. Schematic diagram of Spectral Radiometer discrete filter wheel.  
The central wavelengths of each filter are listed below:

<u>Filter #</u>	<u>Central Wavelength (<math>\mu\text{m}</math>)</u>
3	3.7
6	2.2
7	0.85
8	0.65
9	0.85
10	1.6
11	1.6
12	10.5
(1,2,4,5)	(open)

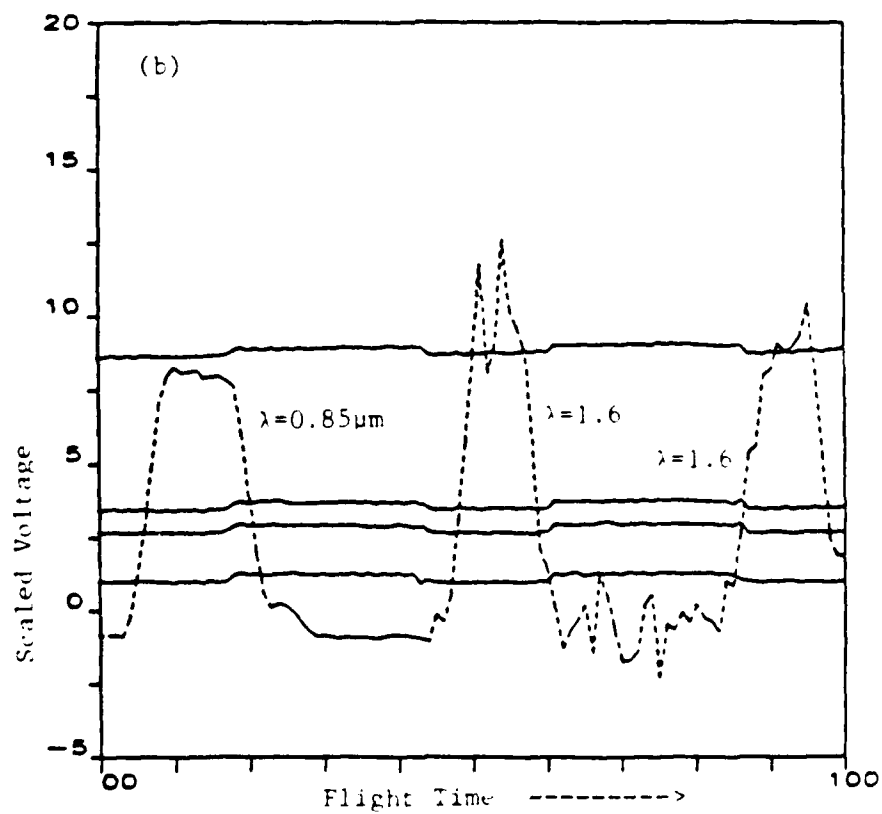
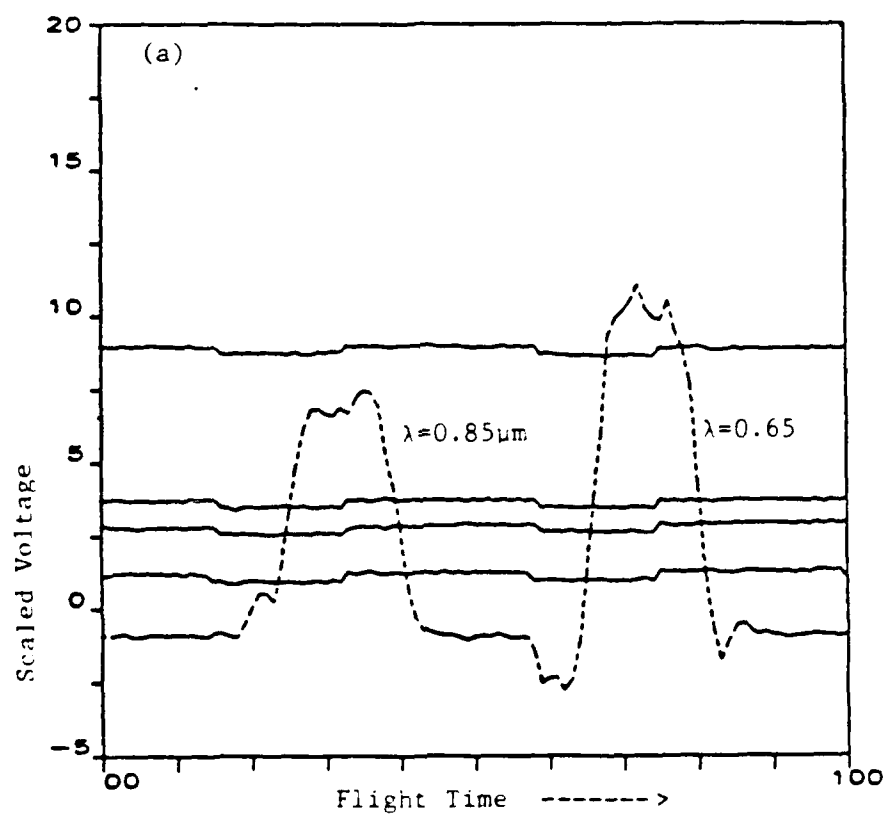


Fig. 16. Spectral radiometer (dotted) and shortwave flux (solid) data for stratus flight studies.

1 072 1 480 2.0 2.0 1 1 18DECC2.IMG 18DECC2

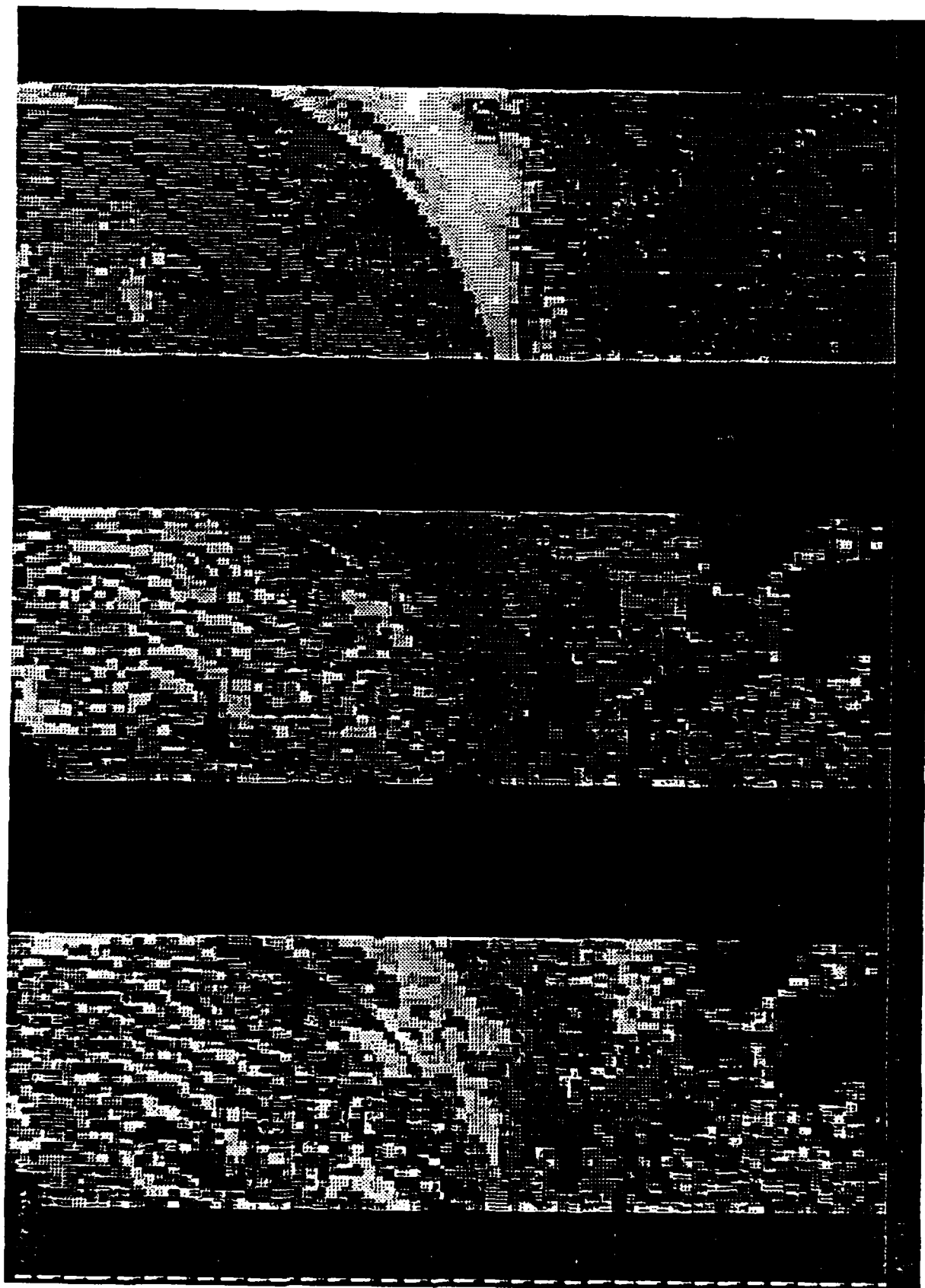


Figure 17. DMSP images in the visible (left), SSC (middle), and infrared (right) channels.

**END  
DATE  
FILMED**

6-18-87

E.A.